49th AIAA Aerospace Sciences Meeting including the New Horizons Forum and Aerospace Exposition
4 - 7 January 2011, Orlando, Florida

AIAA 2011-181

Asymptotic Solutions for Gaseous Flow in a Three-Dimensional Rectangular Microchannel

Khaleel Khasawneh* Hongli Liu† Chunpei Cai‡
New Mexico State University, Las Cruces, New Mexico, 88003-8001

This paper analyzes compressible gaseous flow through a three-dimensional straight uniform rectangular microchannel, and reports a set of asymptotic solutions. This work represents an extension of previous work on compressible flows through a two-dimensional microchannel. First, we choose the ratio of D_h/L as the small expansion parameter, where D_h and L are the channel's hydrodynamic diameter and length correspondingly. Secondly, by comparing the magnitudes of different forces in the compressible gas flow, we obtain a proper criteria to estimate the Reynolds and Mach numbers at the channel exit. We select two sets of Mach and Reynolds numbers and obtain asymptotic analytical solutions of velocities and pressure distributions of compressible gas flow inside the microchannel; and a set of the slip velocity boundary conditions are examined. The analytical results of pressure and velocities are compared with numerical simulation results of the direct simulation Monte Carlo method.

Nomenclature

A	non-dimensional cross section area
A_1, A_2	ratio of hydrodynamic diameter to duct hight and duct width, D_h/H, D_h/W.
A_3	$\sqrt{A_1/A_2}$
A_4	A_1/A_2
D_h	special hydrodynamic diameter, $2WH/(W+H)$, m
H, W	duct height and width, m
k	thermal conductivity, $w/k/m$; or Boltzmann constant
Kn	Knudsen number, λ/D_h
L	duct length, m
M	Mach number
$\dot{m}$	mass flow rate, kg/sec
P	ratio of inlet pressure to outlet pressure, p_i/p_o
p	pressure, Pa
R	gas constant, $J/Kmol$
Re	Reynolds number, $\frac{\rho_o U_o D_h}{\mu}$

*Graduate Student, Department of Mechanical and Aerospace Engineering, Email: kh16867@nmsu.edu.
†Research Associate, Department of Mechanical and Aerospace Engineering, Email: liuhl@nmsu.edu.
‡Assistant Professor, Department of Mechanical and Aerospace Engineering, AIAA Senior Member. Email: ccai@nmsu.edu.

T	temperature, K
u, v, w	velocity components, m/s
$\beta_n(x)$	eigenvalue, $\beta_n(x)\tan(\frac{\beta_n(x)}{2}) = \frac{1}{A_1\theta_u Kn(x)}$
ϵ	ratio of hydrodynamic diameter to duct length, D_h/L
γ	specific heat ratio
γ_m	$2m\pi$
μ	viscosity coefficient, $Pa \cdot sec$
ρ	gas density, kg/m^3
σ_u	momentum accommodation coefficient
θ_u	coefficient, $= (2 - \sigma_u)/\sigma_u$
subscripts	
$_{i,\ o}$	averaged flow property at inlet and outlet
$_{w,\ n,\ t}$	wall, normal and tangent directions on wall
superscript	
$'$	nondimensional property

I. Introduction

MICROCHANNELS are very important components for micro-electro-mechanical systems(MEMS). Some examples of these devices include simple ones such as gas pressure regulators, flow sensors and cooling channels for integrated electronic circuits to complex systems with channels, pumps, valves, sensors and others. Because of the wide applications of these channels, we need to understand the physical laws that govern flows inside these channels, as such we can effectively design and optimize the channels.

In the literature, there is much work on this subject, and here for the literature review we concentrate on gaseous flow inside a straight microchannel. The published experimental tests for the investigations on compressible gas flows in microchannels are relatively rare due to the difficulties involved with the test set-up. Pfalher et al[1] experimentally studied helium and argon gas flows in a trapezoidal microchannel. The measured friction factor was consistently lower than the theoretical predictions. Pong et al.[2] tested nitrogen and helium gas flows in a rectangular microchannel. They suggested that the nonlinear pressure distribution along the microchannel was because of the rarefaction and compressibility effects. Arkilic et al.[3] conducted an analytical and experimental investigation on gaseous flow through long microchannels with slight rarefaction; they derived a two-dimensional theoretical formula for the nonlinear pressure, velocity profiles and mass flow rate of gaseous flow in microchannels. Kavehpour and Faghri[4] studied the gaseous flows in two-dimensional microchannels. They reported that the Nusselt number and friction coefficient were substantially reduced for the slip flow conditions when compared with the continuum flows. Chen[5] studied numerically gas flow in two-dimensional microchannels. The working fluids are nitrogen and helium, and their Knudsen numbers at the channel outlet are 0.055 and 0.165 respectively. The proposed model assumes the fluid is continuum with a slip boundary condition on the channel wall. Chen[6] simulated a three-dimensional steady compressible flow in a microchannel with a reduced form of compressible Navier Stokes equations. He compared calculated mass flow rate and pressure distribution with a known analytical solution for a 2D microchannel flow and experimental data. Chen reported that slip effects played an important role in the friction characteristics of microchannel flow. However, his work was limited to compressible flow under slip condition. Guo and Wu[7] solved the Navier-Stokes equations for gas flows in microtubes and reported similar conclusions. Cai et al.[8] presented a complete set of first-order analytical solutions for a compressible gas flow inside a two-dimensional or axis-symmetric uniform microchannel with a relaxation of the isothermal assumption; their analytic results, including the temperature profiles, agree well with the numerical results.

Sobhan and Garimella[9] conducted a comprehensive study of available experimental data and theoretical investigation results available in the literature on flows and heat transfers in microchannels. They concluded that there was no evidence that the continuum assumptions were violated for the microchannels tested, most of which have hydraulic diameters of 50 μm or more. Yu and Ameel[10] analytically investigated a laminar forced convection in a thermally developing slip flow through isoflux rectangular microchannels by solving the continuum energy equation. Jang and Wereley[11] reported that the pressure inside a rectangular microchannel is nonlinear. Narater and Camberos[12] proposed optimal design with entropy creation, and they adopted gas flows in a microchannel as an example to illustrate the process.

Morini[13] numerically evaluated the trapezoidal and double trapezoidal microchannels and suggested that the Navier-Stokes equations have to be considered valid for microchannels with a hydraulic diameter greater than 30 μm. Hsieh et al.[14]conducted an experimental and theoretical study of low Reynolds number compressible gas flow in a microchannel; his experimental results were found in virtual agreement with those predicted by analytical solutions.

Colin[15] studied the rarefaction and compressibility effects on steady and transient gas flows in microchannels; he summarized the main theoretical and experimental results on steady pressure-driven gas microflows. Lee et al.[16]conducted an experimental investigation to explore the validity of classical correlations based on conventional sized channels to predict the thermal behavior in single-phase flow through rectangular microchannels. Jain and Lin[17] presented numerical results for three-dimensional nitrogen gas flows in microchannels with slip and non-slip boundary conditions. The results agree with the available experimental results. Ebert and Sparrow[18] performed an analysis to determine the velocity and pressure drop in rectangular and annular ducts for rarefied gas flow, and found that the effect of slip is to flatten the velocity distribution relative to that for continuum flow and the axial pressure gradient is diminish under the slip conditions. They found compressibility increases the pressure drop. Guo et al.[19]conducted an experiment to study the flows in two- and three-dimensional microchannels. It was found that a significant pressure drop started at the inlet of the chamber and they predicted an apparent temperature drop at the channel exit.

Numerically, there are other simulation methods for low speed compressible gas flows inside a microchannel as well. For example, there are the Information Preservation (IP) method by Cai et al.,[20] Shen and Fan,[21] gaskinetic BGK method on the higher order of Burnett equation by Xu and Li.[22] Wang et al[23] utilized the Lattice Boltzmann Method (LBM) to simulate the compressible rarefied gas flows in a microchannel.

The objectives of the present work are to obtain a set of asymptotic solutions of velocities and pressure for the compressible gas flow inside a long, uniform, three-dimensional rectangular microchannel using the Navier-Stoke equations.

The following sections are organized as follows: Section II presents the physical problem and the governing equations. Section III analyzes the governing equation for the orders of Reynolds and Mach numbers. Section IV provides a set of asymptotic solutions to this problem. Section V presents validations of the asymptotic solutions. Section VI summarizes this paper with several major conclusions.

II. Physical Problem Description and Governing Equations

The microchannel under consideration has three-dimensions with a height of H, a length of L and a width of W, the origin is set at the center of the channel inlet. Figures (1) and (2) represent the problem under consideration. The average compressible outflow gas properties of pressure, density, temperature, velocity, and number density are $p_o, \rho_o, T_o, U_o, n_o$ respectively, and at the inlet the properties are $p_i, \rho_i, T_i, U_i, n_i$. The inlet pressure is several times larger than the outlet pressure, and the temperature in the flowfield has small variations; hence, a quasi-isothermal assumption is applicable.[8] The averaged outlet quantities are used to normalize the following governing equations and boundary conditions.

In this study, we consider the slip boundary conditions case,[5] $u_w = \theta_u \lambda(x)(\frac{\partial u}{\partial n})_w$ at $y = \pm H/2$ or $z = \pm W/2$ and $v_w = w_w = 0$, where $\theta_u = \frac{2-\sigma_u}{\sigma_u}$, σ_u is the momentum accommodation coefficient, $\lambda(x)$ is the local mean free path at specific cross section.

We normalize the flow properties with the averaged values at the channel exit: $p_o, \rho_o, T_o, U_o, n_o$, and x, y, z coordinates with the channel length, height and width, L, H, W, and adopt the superscript ($'$) to denote the nondimensional quantities. If we denote $D_h = \frac{2WH}{W+H}$, where D_h is the hydrodynamic diameter, with the quasi-isothermal condition, we can assume that the viscosity coefficient μ and the heat conductivity

k are constant, then the nondimensional governing equations are:

$$\epsilon\frac{\partial(\acute{\rho}\acute{u})}{\partial\acute{x}}+A_1\frac{\partial(\acute{\rho}\acute{v})}{\partial\acute{y}}+A_2\frac{\partial(\acute{\rho}\acute{w})}{\partial\acute{z}}=0 \tag{1}$$

$$\epsilon\acute{\rho}\acute{u}\frac{\partial\acute{u}}{\partial\acute{x}}+A_1\acute{\rho}\acute{v}\frac{\partial\acute{u}}{\partial\acute{y}}+A_2\acute{\rho}\acute{w}\frac{\partial\acute{u}}{\partial\acute{z}}=-\frac{\epsilon}{\gamma M^2}\frac{\partial\acute{p}}{\partial\acute{x}}+\frac{1}{Re}\left[\epsilon^2\frac{\partial^2\acute{u}}{\partial\acute{x}^2}+A_1^2\frac{\partial^2\acute{u}}{\partial\acute{y}^2}+A_2^2\frac{\partial^2\acute{u}}{\partial\acute{z}^2}+\frac{1}{3}\left(\epsilon^2\frac{\partial^2\acute{u}}{\partial\acute{x}^2}+\epsilon A_1\frac{\partial^2\acute{v}}{\partial\acute{x}\partial\acute{y}}+\epsilon A_2\frac{\partial^2\acute{w}}{\partial\acute{x}\partial\acute{z}}\right)\right] \tag{2}$$

$$\epsilon\acute{\rho}\acute{u}\frac{\partial\acute{v}}{\partial\acute{x}}+A_1\acute{\rho}\acute{v}\frac{\partial\acute{v}}{\partial\acute{y}}+A_2\acute{\rho}\acute{w}\frac{\partial\acute{v}}{\partial\acute{z}}=-\frac{A_1}{\gamma M^2}\frac{\partial\acute{p}}{\partial\acute{y}}+\frac{1}{Re}\left[\epsilon^2\frac{\partial^2\acute{v}}{\partial\acute{x}^2}+A_1^2\frac{\partial^2\acute{v}}{\partial\acute{y}^2}+A_2^2\frac{\partial^2\acute{v}}{\partial\acute{z}^2}+\frac{1}{3}\left(\epsilon A_1\frac{\partial^2\acute{u}}{\partial\acute{x}\partial\acute{y}}+A_1^2\frac{\partial^2\acute{v}}{\partial\acute{y}^2}+A_1A_2\frac{\partial^2\acute{w}}{\partial\acute{y}\partial\acute{z}}\right)\right] \tag{3}$$

$$\epsilon\acute{\rho}\acute{u}\frac{\partial\acute{w}}{\partial\acute{x}}+A_1\acute{\rho}\acute{v}\frac{\partial\acute{w}}{\partial\acute{y}}+A_2\acute{\rho}\acute{w}\frac{\partial\acute{w}}{\partial\acute{z}}=-\frac{A_2}{\gamma M^2}\frac{\partial\acute{p}}{\partial\acute{z}}+\frac{1}{Re}\left[\epsilon^2\frac{\partial^2\acute{w}}{\partial\acute{x}^2}+A_1^2\frac{\partial^2\acute{w}}{\partial\acute{y}^2}+A_2^2\frac{\partial^2\acute{w}}{\partial\acute{z}^2}+\frac{1}{3}\left(\epsilon A_2\frac{\partial^2\acute{u}}{\partial\acute{x}\partial\acute{z}}+A_1A_2\frac{\partial^2\acute{v}}{\partial\acute{y}\partial\acute{z}}+A_2^2\frac{\partial^2\acute{w}}{\partial\acute{z}^2}\right)\right] \tag{4}$$

$$\acute{p}=\acute{\rho}\acute{T}=\acute{n}\acute{T} \tag{5}$$

The non-dimensional wall boundary conditions at $\acute{y}=\pm1/2$ or $\acute{z}=\pm1/2$ are: $\acute{u}_w=\theta_uKn(\acute{x})F(\frac{\partial\acute{u}}{\partial n})_w$, $\acute{v}_w=\acute{w}_w=0$ for the slip velocity boundary condition, where $Kn(\acute{x})=Kn_o/\rho_1(\acute{x})$ and $F=A_1$ or $F=A_2$ for the y or z direction respectively.

III. Order Analysis for Reynolds and Mach Numbers at Channel Exit

A proper order estimation can greatly simplify the problem. Following the work by Cai et al,[8] we apply the X-momentum equation for the whole channel, and obtain the following equation regarding the outlet Mach and Reynolds numbers:

$$\frac{1}{4}(p_o-p_i)\pi D_h^2+\frac{1}{4}\rho_ou_o\pi D_h^2(u_o-u_i)+L\pi D_h\mu(\frac{u_o}{D_h}+\frac{u_i}{D_h})\sim0 \tag{6}$$

where $\frac{1}{4}(p_o-p_i)\pi D_h^2$ is the pressure drop, $\frac{1}{4}\rho_ou_o\pi D_h^2(u_o-u_i)$ is the momentum change, and $L\pi D_h\mu(\frac{u_o}{D_h}+\frac{u_i}{D_h})$ is the averaged shear stress along the wall surface. If we assume u_i and u_o on the same order and denote $P=p_i/p_o$ for the pressure ratio, we can obtain:

$$O[(P-1)\epsilon M^{-2}]-O[\gamma\epsilon]-O[\gamma/Re]\sim0 \tag{7}$$

In Eqn.(7), there are four possible combinations for the Mach and Reynolds numbers among the three terms: any two of these three terms are on the same order, so they balance each other; or all of these three terms are of the same order. This equation of the Mach and Reynolds numbers illustrates that we cannot randomly choose the orders for them. Some people suggest choosing these numbers as shown in Table 1; however, as we can see, only three of the combinations can provide proper balance of the forces. Some unrealistic combinations in the table can even provide hypersonic results. Meanwhile, we must be aware that there are more feasible combinations which are not included in Table 1. As long as they satisfy the above governing relation, they are proper parameters to simplify Eqns. (1-5).

In this paper, we are interested in low speed gas flows, and we choose the following two cases: $M\sim O(\epsilon)$, $Re\sim O(\epsilon)$ and $M\sim O(\epsilon^{1/2})$, $Re\sim O(1)$ for our analysis. The later combination of parameters is not listed in Table 1 but it satisfies the above governing equation.

IV. Asymptotic Solutions For Slip Velocity Boundary Conditions

We choose the coordinate origin at the center of the inlet cross section, and we choose the flow direction as the x-axis. Because u_1 is symmetric about the centerline, we can consider only the right-top quarter of the cross section to simplify the problem. For simplicity, the superscripts ($'$) for the nondimensional formats in Eqns (1-5) are removed in the following sections, hence all the variables are in non-dimensional forms.

We define the following formats for the non-dimensional quantities:

$$\begin{aligned} &u = u_1 + \epsilon u_2 + \epsilon^2 u_3 + ..., \quad v = v_1 + \epsilon v_2 + \epsilon^2 v_3 + ..., \quad w = w_1 + \epsilon w_2 + \epsilon^2 w_3 + ..., \quad p = p_1 + \epsilon p_2 + ..., \\ &\rho = \rho_1 + \epsilon \rho_2 + \epsilon^2 \rho_3 + ..., \quad n = n_1 + \epsilon n_2 + \epsilon^2 n_3 + ..., \quad T = 1 + \epsilon T_2 + \epsilon^2 T_3 + ... \end{aligned} \tag{8}$$

For the flowfield in the microchannel, pressure and density change rapidly, whereas temperature does not change significantly. As such, it is reasonable to use the quasi-isothermal condition, i.e., the leading term of T is unity. Consequently, we can assume that the viscosity coefficient μ and the heat conductivity k are constant. By expanding and separating terms of different magnitudes in Eqn.(1), and further introducing a potential function ϕ for v_1 and w_1, we obtain the following relation from the continuity equation:

$$\epsilon^0 : A_1 \frac{\partial v_1}{\partial y} + A_2 \frac{\partial w_1}{\partial z} = A_1 \frac{\partial^2 \phi}{\partial y^2} + A_2 \frac{\partial^2 \phi}{\partial z^2} = 0 \tag{9}$$

With the $v_1 = w_1 = 0$ as the boundary conditions, we can conclude, ϕ is a constant along the boundary. As such, we obtain a trivial solution of constant ϕ and hence $v_1 = w_1 = 0$.

We can obtain the solutions of u_1, v_2, and w_2 by considering the leading terms in the x, y and z-momentum equations. From the y- and z- momentum Eqns, the leading term is $O(\frac{1}{\epsilon^2})$ and it provides relations that $\frac{\partial p_1}{\partial y} = 0$, $\frac{\partial p_1}{\partial z} = 0$, i.e, p_1 is a function of x only. The leading term in the x-momentum Eqn.(2) is:

$$A_1^2 \frac{\partial^2 u_1}{\partial y^2} + A_2^2 \frac{\partial^2 u_1}{\partial z^2} = \frac{\epsilon Re}{\gamma M^2} \frac{dp_1}{dx} \tag{10}$$

We denote the right hand side term as $c_1(x)$ hereafter. The asymptotic solution of u_1 at a specific cross section can be derived from Eqn.(10) with constant $c_1(x)$, and the solutions of $v_2(x, y, z)$ and $w_2(x, y, z)$ can be derived by substituting Eqn.(8) into Eqn.(1) and using the condition that $p_1 = \rho_1$. By collecting terms of order ϵ^1, we obtain:

$$A_1 \frac{\partial v_2}{\partial y} + A_2 \frac{\partial w_2}{\partial z} = -\frac{dp_1}{p_1 dx} u_1 - \frac{\partial u_1}{\partial x} \tag{11}$$

where the right hand side term is defined as $S_1(x, y, z)$. From the above Eqn.(11) we can solve for v_2 and w_2 by computing the source term containing u_1 and applying the wall boundary conditions. The most convenient approach probably is to introduce a new potential function, $v_2 = \partial\phi_2/\partial y$ and $w_2 = \partial\phi_2/\partial z$:

$$A_1 \frac{\partial^2 \phi_2}{\partial y^2} + A_2 \frac{\partial^2 \phi_2}{\partial z^2} = S_1(x, y, z) \tag{12}$$

along the tangent and normal direction of the boundary, the gradients of ϕ_2 is zero. As such, a general Poisson's equation is obtained with proper boundary conditions.

The u_1 solution can be derived from Eqn.(10) with the following boundary conditions:

$$\begin{aligned} &\tfrac{\partial u(x,y,z)}{\partial y} = 0, \text{at y} = 0; \quad u_w(x, 1/2, z) = -\theta_u Kn(x) A_1 (\tfrac{\partial u(x,y,z)}{\partial y})_{y=1/2}; \\ &\tfrac{\partial u(x,y,z)}{\partial z} = 0, \text{at z} = 0; \quad u_w(x, y, 1/2) = -\theta_u Kn(x) A_2 (\tfrac{\partial u(x,y,z)}{\partial z})_{z=1/2}; \end{aligned} \tag{13}$$

using the solution in Ozisik[24] for a similar partial differential equation, we obtain:

$$u_1(x, y, z) = \theta(x, y, z) + \frac{c_1(x)}{2A_1^2} y^2 - \frac{c_1(x)}{8A_1^2} [4A_1 \theta_u Kn(x) + 1] \tag{14}$$

The governing equation for $\theta(x, y, z)$ has one non-homogenous boundary condition at $z = 1/2$, as such it can be solved by the separation of variables method in Kreyzig.[25] The solution of $\theta(x, y, z)$ is:

$$\theta(x, y, z) = c_1(x) \sum_{n=1,2,..}^{\infty} D_n(x) \cosh(A_4 \beta_n(x) z) \cos(\beta_n(x) y) \tag{15}$$

where $\beta_n(x) \tan(\frac{1}{2}\beta_n(x)) = \frac{1}{A_1 \theta_u Kn(x)}$, $D_n(x)$ is given by:

$$D_n(x) = \frac{4 \sin(\frac{\beta_n(x)}{2})}{A_1^2 \beta_n^2 [A_1 \beta_n(x) \theta_u Kn(x) \sinh(\frac{1}{2} A_4 \beta_n(x)) + \cosh(\frac{1}{2} A_4 \beta_n(x))]} \frac{1}{\sin \beta_n(x) + \beta_n(x)} \tag{16}$$

then the solution of $u_1(x,y,z)$ for $0 \le y \le 1/2$ and $0 \le z \le 1/2$ is:

$$u_1(x,y,z) = c_1(x)\Big[\sum_{n=1,2,..}^{\infty} D_n(x)\cosh[A_4\beta_n(x)z]\cos[\beta_n(x)y] + \frac{4y^2 - 1 - 4A_1\theta_u Kn(x)}{8A_1^2}\Big] \tag{17}$$

For other three quadrants, the solutions are symmetric to the above one for the first quadrant.

The solutions of $v_2(x,y,z)$ and $w_2(x,y,z)$ for the slip case are obtained by solving the following equation:

$$A_1\frac{\partial v_2}{\partial y} + A_2\frac{\partial w_2}{\partial z} = S_2(x,y,z) = \Big(-\frac{1}{p_1}\frac{dp_1}{dx} - \frac{\partial}{\partial x}\Big)u_1 = k(x)u_1(x,y,z) \tag{18}$$

where $u_1(x,y,z)$ is known, $k(x) = \Big(-\frac{1}{p_1}\frac{dp}{dx} - \frac{\partial}{\partial x}\Big)$ is a mathematical operator. The simplest approach to solve the above equation is to introduce a simple potential function. It can be proved that the final expressions for the $v_2(x,y,z)$, $w_2(x,y,z)$ solutions are:

$$v_2(x,y,z) = -\sum_{m=1,2,3,..}^{\infty} \gamma_m\Big(E_m(x)\cosh(A_3\gamma_m z) + Z_m(x,z)\Big)\sin(\gamma_m y) \tag{19}$$

$$w_2(x,y,z) = \sum_{m=1,2,3,..}^{\infty} \Big(A_3\gamma_m E_m(x)\sinh(A_3\gamma_m z) + \frac{\partial Z_m(x,z)}{\partial z}\Big)\cos(\gamma_m y) \tag{20}$$

where:

$$E_m(x) = 4k(x)c_1(x)\sum_{n=1,2,...}^{\infty} D_n(x)l_{nm}(x)\frac{A_4\beta_n(x)}{A_2A_3\gamma_m(A_3^2\gamma_m^2 - A_4^2\beta_n(x)^2)}\frac{\sinh(\frac{1}{2}A_4\beta_n(x))}{\sinh(\frac{1}{2}A_3\gamma_m)} \tag{21}$$

$$Z_m(x,z) = -2k(x)c_1(x)\Big[\frac{(-1)^m}{A_1^3\gamma_m^4} + 2\sum_{n=1,2,..}^{\infty} D_n l_{nm}\Big(\frac{1}{A_2(A_3^2\gamma_m^2 - A_4^2\beta_n^2(x))}\Big)\cosh(A_4\beta_n(x)z)\Big] \tag{22}$$

$$\frac{\partial Z_m(x,z)}{\partial z} = -4k(x)c_1(x)\frac{A_4}{A_2}\sum_{n=1,2,..}^{\infty} D_n(x)l_{nm}(x)\Big(\frac{\beta_n(x)}{A_3^2\gamma_m^2 - A_4^2\beta_n^2(x)}\Big)\sinh[A_4\beta_n(x)z] \tag{23}$$

$$l_{nm}(x) = \frac{-\beta_n(x)}{\beta_n^2(x) - \gamma_m^2}\sin(\frac{\beta_n(x)}{2}), \tag{24}$$

One result is evident: that v_2 is an odd function about the y-axis, and w_2 is an odd function about the z-axis.

The analytical solution of the mass flow rate $\dot{m}$ can be derived at a different cross section using the analytical solution of $u_1(x,y,z)$ for that section, with the averaged velocity u_{1m}:

$$u_{1m}(x) = 4c_1(x)\Big(\frac{1}{A_4}\sum_{n=1,2,3,..}^{\infty}\Big[\frac{D_n(x)}{\beta_n^2(x)}\sinh(\frac{1}{2}A_4\beta_n(x))\sin(\frac{1}{2}\beta_n(x))\Big] - \frac{1}{8A_1^2}(A_1\theta_u Kn(x) + \frac{1}{6})\Big) \tag{25}$$

Since $\rho_1 = p_1$, and the x value is specified at the channel exit where pressure is equal to one, then $\dot{m}$ is:

$$\dot{m} = 4p_1(x)c_1(x)\Big(\frac{1}{A_4}\sum_{n=1,2,3,..}^{\infty}\Big[\frac{D_n(x)}{\beta_n(x)^2}\sinh(\frac{1}{2}A_4\beta_n(x))\sin(\frac{1}{2}\beta_n(x))\Big] - \frac{1}{8A_1^2}(A_1\theta_u Kn(x) + \frac{1}{6})\Big) = m_o \tag{26}$$

The pressure distribution is obtained from the above equation, with the following format:

$$Q_1\frac{dp_1^2}{dx} - \frac{\theta_u Kn_o}{4A_2}\frac{dp_1}{dx} = Q_2 \tag{27}$$

where Q_2 is a coefficient related to the mass flow rate, and

$$Q_1 = \sum_{n=1,2,3,..}^{\infty}\Big[\frac{4\sin^2\frac{\beta_n(x)}{2}}{A_1^2\beta_n^4\big[A_1\beta_n\theta_u Kn(x) + \coth(\frac{1}{2}A_4\beta_n)\big]}\frac{1}{\sin\beta_n + \beta_n}\Big] - \frac{1}{48A_1A_2} \tag{28}$$

It should be noted that Q_1 implicitly contains $p_1(x)$ through $\beta_n(x)$. With the pressure values at the inlet and outlet, the solution to Eqn. (27) is:

$$p_1(x) = \frac{\frac{\theta_u Kn_o}{4A_2} - \sqrt{(\frac{\theta_u Kn_o}{4A_2})^2 + 4Q_1[Q_1(1-P^2) - (1-P)\frac{\theta_u Kn_o}{4A_2}]x + 4Q_1^2P^2 - PQ_1\frac{\theta_u Kn_o}{A_2}}}{2Q_1} \tag{29}$$

Because Q_1 contains $p_1(x)$ through $\beta_n(x)$, solving for p_1 with the above equation requires an iterative procedure. A simpler approach is to integrate Eqn.(27) over x, then we can choose pressure value and solve for the corresponding x. Obviously, this approach avoids the iterative process.

If we consider the two-dimensional case as the limiting case with the largest ratio of width/height, and a circular cross section as the other limiting case of unit cross section ratio, then some past work[8] indicates that there is very insignificant difference between these two limits.

Friction factor f and Reynolds number Re for the slip velocity boundary condition case are:

$$f = \left(-\frac{dp}{dx}\right)\frac{2D_h}{\rho_1 u_{1m}^2(x)}; Re = \frac{\rho_1 u_{1m}(x) D_h}{\mu} \tag{30}$$

in the above equation the terms in the right hand side of f and Re are dimensional, the above equations yield the following formula for the Poiseuille number P_o:

$$P_o = -\frac{1}{2}\frac{1}{\frac{1}{A_4}\sum_{n=1,2,3,..}^{\infty}\left[\frac{D_n(x)}{\beta_n(x)^2}\sinh(\frac{1}{2}A_4\beta_n(x))\sin(\frac{1}{2}\beta_n(x))\right] - \frac{1}{8A_1^2}(A_1\theta_u\frac{Kn_o}{p_1(x)} + \frac{1}{6})} \tag{31}$$

Obviously, the above P_o number is a function of aspect ratio W/H, pressure ratio P, outlet Knudsen number Kn_o and the normalized position x.

V. Validation and Results

To validate the above analytical results, we simulate two finite length uniform microchannel flows with a specific particle simulation package named GRASP,[26] which is developed at New Mexico State University. This method is different than solving the Navier-Stokes Equations. However, even though some discrepancies are expected, we anticipate the DSMC simulation results to be close to the analytical solutions.

For the first test case, we adopt one benchmark case which is similar to a test case in another paper.[8] We assume oxygen gas flows through a microchannel with a length of 15 μm, a width and a height of 0.53 μm. The pressure ratio is 2.5, the outlet pressure is 1 atm, the temperatures for the inlet, outlet, and wall are 300 Kelvin, and the power law is adopted to compute the viscosity.

Figure (3) shows the centerline U-velocity distributions. The U-velocity increases along the x-axis, and the DSMC results are close to the average value of the two sets of analytical results. At the middle of the channel the difference between the DSMC and the analytical solution is about 15%. We point out that the analytical centerline U-velocity is very close to that from the round tube cross section case with a tube diameter of 0.53 μm.[8]

Figure (4) shows the normalized centerline pressure distributions. It is clear that the analytical results with the slip velocity boundary conditions agree well with the DSMC results. The pressure gradient at the inlet is small but it increases toward the exit. This is because the low wall friction allows higher U-velocity and requires lower density, because the continuity equation has to be satisfied.

Figure (5) shows the contours of U-velocity in the Z=0 plane for the analytical solution and the DSMC results. The results have the same trends with large gradients at the channel exit. Figure (6) shows the U-velocity contours at the middle station, $x/L = 0.5$, for slip velocity boundary conditions, the results have very close values.

Figures (7) - (10) show the results for another test case, with a channel width of 1.06 μm, and a height of 0.53 μm, other properties are the same as the first case. The trends are similar to the previous case but some different patterns appear. For example, the velocity profiles are effected by the larger aspect ratio.

The discrepancy in the analytical and the DSMC results are due to the following reasons: First, the boundary treatment in the DSMC simulations can result in some differences. If we include a second order velocity slip model for the wall boundary condition, we may obtain improved analytical results from the

DSMC simulation. The inlet and outlet setup for the DSMC simulation contributes to the major differences, because in the DSMC simulations, flow adjusts from a free, uniform flow to a tube flow at the inlet; while the analytical results do not include such entrance effects. Further, at the outlet, the gradients are large, any numerical treatment of outlet flow may have some effects. However, for the analytical results, no such inlet and outlet effects are considered, we assume the results are valid for a section of the channel flow. Secondly, the U-velocity profiles are functions of pressure gradients. There are some pressure differences between the DSMC and analytical results, for such a small length scale, any small difference in pressure result in large pressure gradients. As such, it is not surprising to observe some discrepancies among the DSMC and analytical results.

VI. Summary

We have presented a set of asymptotic solutions for the compressible gas flowfield inside a three-dimensional straight microchannel with a uniform rectangular cross section. In summary, the following results are obtained:

1) By comparing the different forces, i.e., the viscous force, the pressure drop, and the momentum change, we have obtained a fundamental relation, Eqn.(7), which links the Mach and Reynolds numbers at the channel exit, the pressure ratio P, and the channel geometry ratio ϵ. This relation provides a guideline to choose different Reynolds and Mach number orders to simplify the Navier-Stokes Equations. In this paper, we have choose two combinations of orders of Reynolds and Mach numbers, $M \sim O(\epsilon)$, $Re \sim O(\epsilon)$ and $M \sim O(\epsilon^{1/2})$, $Re \sim O(1)$. The asymptotic solutions are valid for these two cases.

2) We have provided the full solutions of u_1, v_2, w_2, and p_1 with slip velocity boundary conditions. To the authors' best knowledge, these are the most complete set of solutions obtained in the literature, they can serve as the benchmark test cases for further studies. For the pressure distribution, the format is slightly different from those obtained in the literature. By assuming specific pressure values then solve for the station values of x, we avoid the complex iterative procedure. There are some basic properties about the v_2 and w_2 expressions, for example, v_2 is an odd function about the y-axis, and w_2 is an odd function about z-axis.

3) We have compared the analytical results against some numerical results from the DSMC simulation. The numerical results show the same trends with the asymptotic solutions we obtained. For example, the centerline pressure and velocity profiles, the u-velocity contours along the streamwise directions, and at the middle sections.

Acknowledgement

We gratefully acknowledge the support from the National Science Foundation grant CBET-0854411.

References

[1]Pfalher, J., Harley, J., Bau, H., and Zemel, J., "Gas And Liquid Flow in Small Channels," *ASME DSC Symp. on Micromechanical Sensors, Actuators, and Systems*, Vol. 32, May, 1991, pp. 49-60.

[2]Pong, K., Ho, C., Liu, J., and Tai, H., "Non-linear Pressure Distribution in Uniform Microchannels," *ASME FED Application of Microfabrication to Fluid Mechanics*, Vol. 197, May, 1994, pp. 51-56.

[3]Arkilic, E., Schmidt, K. and Breuer, K.,"Gaseous Slip Flow in Long Microchannels," *Journal of Microelectromechanical Systems*, Vol. 6, No. 2, 1997, pp. 167-178.

[4]Kavehpour, H. and Faghri, M., "Effects of Compressibility and Rarefaction on Gaseous Flows in Microchannels," *Journal of Numerical Heat Transfer*, Vol. 32, No. 7, 1997, pp. 677-695.

[5]Chen, C., Lee, M. and Sheu, J., "Numerical Analysis of Gas Flow in Microchannels," *J. Numerical Heat Transfer*, Vol. 33, No.7, 1998, pp.749-762.

[6]Chen, C., "Numerical Method for Predicting Three-Dimensional Steady Compressible Flow in Long Microchannels," *J. Micromechanics and Microengineering*, Vol. 14, June, 2004, pp. 1091-1100.

[7]Guo, Z. and Wu, X., "Compressibility Effects on The Gas Flow And Heat Transfer In A Micro Tube," *International Journal Heat and Mass Transfer*, Vol. 40, No. 2, 1997, pp. 3251–4.

[8]Cai, C., Sun, Q. and Boyd, I., "Gas Flows in Microchannels and Microtube," *Journal of Fluid Mechanics*, Vol. 589, August, 2007, pp. 305-314.

[9]Sobhan, C. and Garimella, S., "A Comparative Analysis of Studies On Heat Transfer And Fluid Flow in Microchannels," *Journal of Microscale Thermophysics*, Vol. 5, No. 4, 2001, pp. 293-311.

[10]Yu, S., Ameel, T., "Slip Flow Convection in Isoflux Rectangular Microchannels," *Journal of Heat Transfer*, Vol. 124, No. 2, 2002, pp. 346 - 355.

[11]Jang, J. and Wereley, S.T., "Pressure Distributions of Gasesous Slip Flow in Straight and Uniform Rectangular Microchannels," *Microfluid NanoFluid*, Vol. 1, August, 2004, pp. 41-51.

[12]Naterer, G.F. and Camberos, J.A., *Entropy Based Design and Analysis of Fluid Engineering Systems*, CRC Press, Boca Raton, February, 27, 2008.

[13]Morini, G.,"Single-Phase Convective Heat Transfer In Microchannel: A Review of Experimental Results," *International Journal of Thermal Sciences*, Vol. 43, No. 7, 2004, pp. 631-651.

[14]Hsieh, S., Tsai, H., Lin, C., Huang, C. and Chien, C.,"Gas Flow in Long Microchannels," *International Journal of Heat and Mass Transfer*, Vol. 47, No. 17-18, 2004, pp. 3877–87.

[15]Colin, S., "Rarefaction and Compressiblity Effects on Steady and Trasint Gas Flows in Microchannels," *Journal of Microfluid and Nanofluid*,Vol. 1, No. 3, 2005, pp. 268-279.

[16]Lee, P., Garimella, S. and Liu, D., "Investigation of Heat Transfer in Rectangular Microchannels," *International Journal of Heat and Mass Transfer*, Vol. 48, No. 9, 2005, pp. 1688-1704.

[17]Jain, V. and Lin, C., "Numerical Modeling of Three-Dimensional Compressible Gas Flow In Microchannnels," *Journal of Micromechanics and Microengineering*, Vol. 16, Jan., 2006, pp. 292-302.

[18]Ebert, W. and Sparrow, E., "Slip Flow in Rectangular and Annular Ducts ," *J. Basic Engineering*, Vol. 87, December, 1965, pp. 1018-1024.

[19]Guo, X., Huang, C., Alexeenko, A., and Sullivan, J., "Numerical And Experimental Study of Gas Flows in 2D and 3D Microchannels," *Journal of Micromechanics and Microengineering*, Vol. 18, No. 2, 2008, pp. 1-8.

[20]Cai, C., Boyd, I.D., Fan, J., and Candler, G.V., "Direct Simulation Methods for Low-Speed Microchannel Flows," *Journal of Thermophysics and Heat Transfer*, Vol. 14, No. 3, July-September, 2000, pp. 368-378.

[21]Shen, C., Fan, J., and Xie, C., "Statistical Simulation of Rarefied Gas Flows in Micro-Channels," *Journal of Computational Physics*, Vol. 189, Issue 2, August 2003, pp. 512-526.

[22]Xu, K. and Li, Z., "Microchannel Flow in The Slip Regime: Gas-kinetic BGK-Burnett Solutions," *Journal of Fluid Mechanics*, 513, April, 2004, pp. 87-110.

[23]Wang, M. and Li, Z., "Micro- and Nanoscale Non-Ideal Gas Poiseuille Flows in A Consistent Boltzmann Algorithm Model," *Journal of MicroMechanics and Microengineering*, 14, June 2004, pp. 1057–1063.

[24]Ozisik, M., *Heat Conduction,* John Wiley and Sons, New York, 1980, pp. 67-69, 632-634.

[25]Kreyzig, E., *Advanced Engineering Mathematics,* John Wiley and Sons, New York, 2006.

[26]Liu, H and Cai, C., "An Object-Oriented Serial DSMC Simulation Package," 27th International Rarefied Gasdynamics Symposium, Pacific Grove, CA, July 10-15, 2010.

Table 1. Order Estimations for Different Mach and Reynolds Number Combinations.

$\frac{(P-1)\epsilon}{M^2} : \gamma\epsilon : \frac{\gamma}{R}$	$R \sim O(\epsilon)$	$R \sim O(1)$	$R \sim O(1/\epsilon)$
$M \sim O(\epsilon)$	$\left[\ \frac{P-1}{\epsilon} : \gamma\epsilon : \frac{\gamma}{\epsilon}\ \right]$	$\frac{P-1}{\epsilon} : \gamma\epsilon : \gamma$	$\frac{P-1}{\epsilon} : \gamma\epsilon : \gamma\epsilon$
$M \sim O(1)$	$(P-1)\epsilon : \gamma\epsilon : \frac{\gamma}{\epsilon}$	$(P-1)\epsilon : \gamma\epsilon : \gamma$	$\left[\ (P-1)\epsilon : \gamma\epsilon : \gamma\epsilon\ \right]$
$M \sim O(1/\epsilon)$	$(P-1)\epsilon^3 : \gamma\epsilon : \frac{\gamma}{\epsilon}$	$(P-1)\epsilon^3 : \gamma\epsilon : \gamma$	$\left[\ (P-1)\epsilon^3 : \gamma\epsilon : \gamma\epsilon\ \right]$

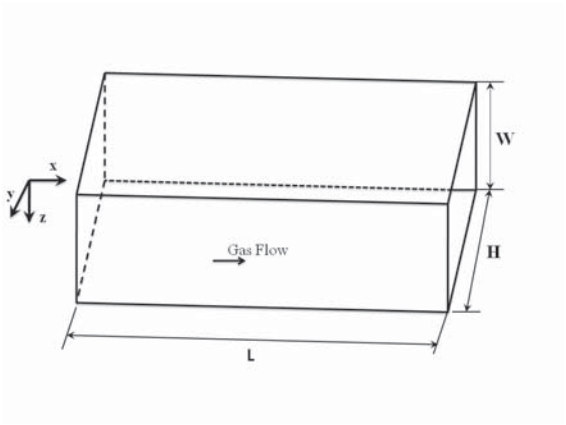

Figure 1. Illustration of the problem(not in scale).

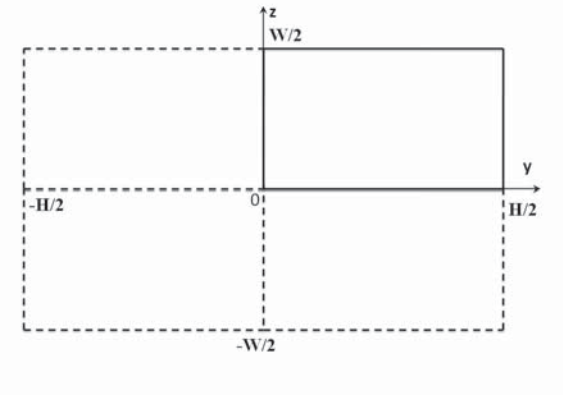

Figure 2. Cross section of the duct.

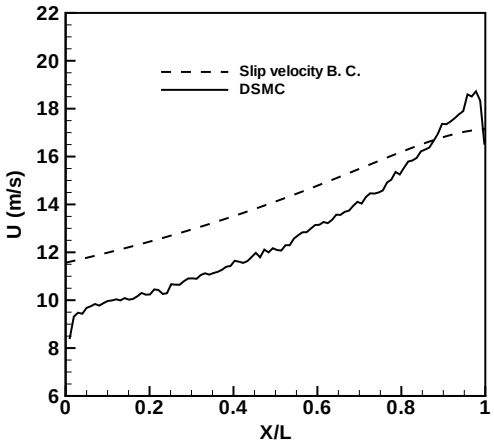

Figure 3. Center line U-velocity along flow direction (m/s), W = H = 0.53 μm, L=15 μm, O_2.

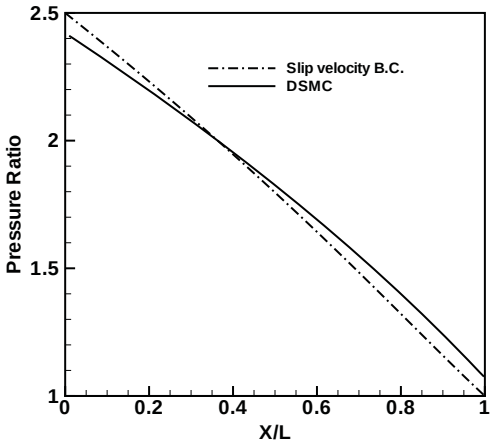

Figure 4. Normalized centerline pressure distribution, W = H = 0.53 μm, L = 15 μm, O_2.

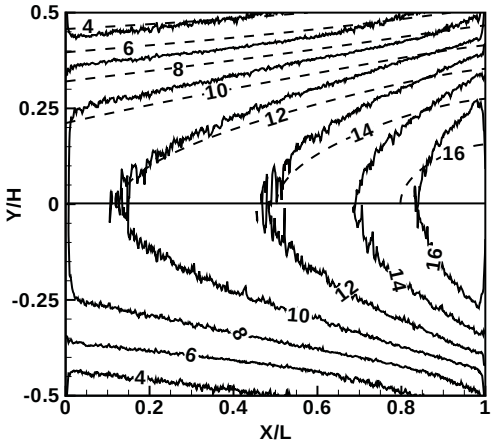

Figure 5. U-velocity contours (m/s) in plane $z = 0$, solid: DSMC, dashed: slip velocity B.C.s, W = H= 0.53 μm, L = 15 μm, O_2.

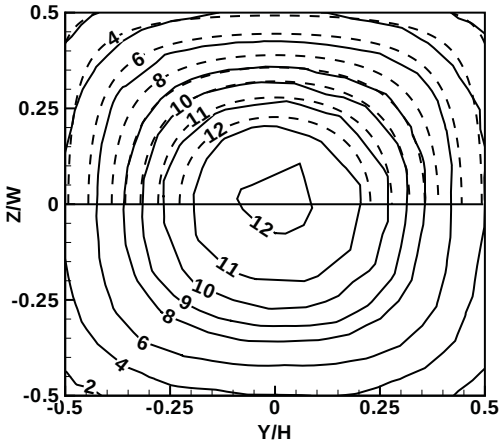

Figure 6. U-velocity contours (m/s) at x/L=0.5, solid: DSMC, dashed: slip velocity B.C.s. W = H= 0.53 μm, L = 15 μm, O_2.

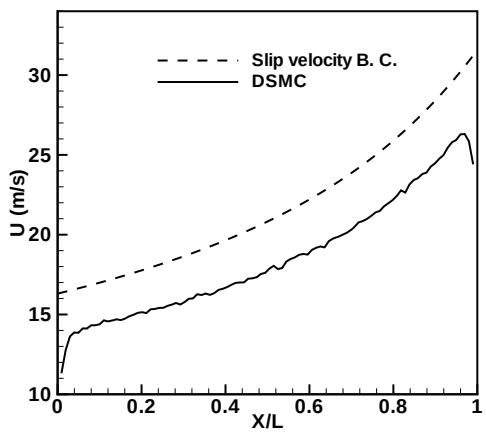

Figure 7. Centerline U-velocity (m/s) profiles, W = 1.06 μm, H = 0.53 μm, L=15 μm, O_2.

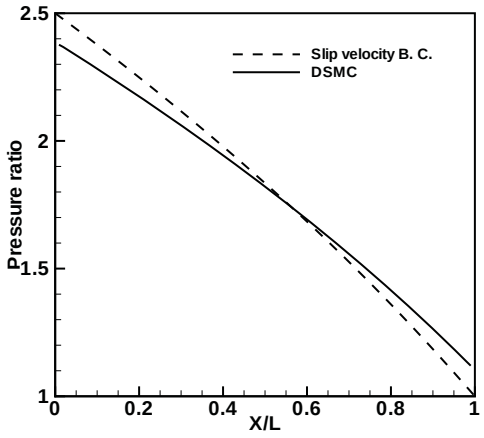

Figure 8. Centerline pressure distributions, W = 1.06 μm, H = 0.53 μm, L = 15 μm, O_2.

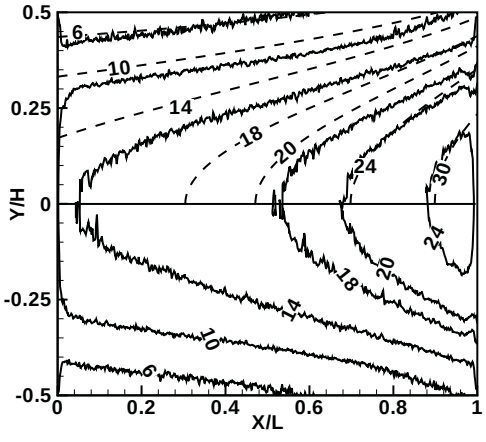

Figure 9. U-velocity contours (m/s) in plane $z = 0$, solid: DSMC, dashed: slip velocity B.C.s, W = 1.06 μm, H= 0.53 μm, L = 15 μm, O_2.

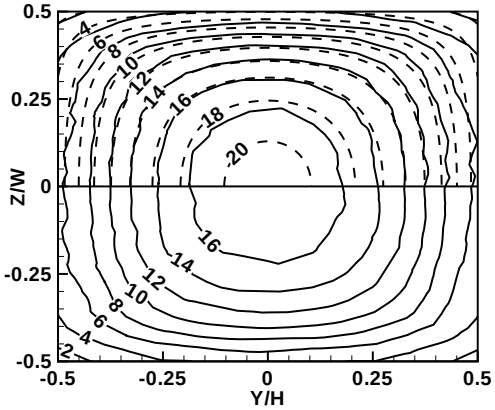

Figure 10. U-velocity contours (m/s) at x/L=0.5, solid: DSMC, dashed: slip velocity B.C.s, W = 1.06 μm, H= 0.53 μm, L = 15 μm, O_2.